Upcycling cellulose waste textile into aerogel beads via prilling technique

Marion Négrier, Elise El Ahmar, Romain Sescousse, Martial Sauceau, Guenaelle Bouet, David Eglin, Tatiana Budtova

Upcycling cellulose waste textile into aerogel beads via prilling technique

Marion Negrier · Elise El Ahmar · Romain Sescousse · Martial Sauceau · Guenaelle Bouet · David Eglin · Tatiana Budtova

Abstract The goal is to demonstrate the possibility of upcycling waste textile into high value-added materials, aerogels. Prilling (or jet-vibration) method was used to make aerogel beads based on viscose textile and also on microcrystalline cellulose (MCC), the latter used as a reference. The solvent was ionic liquid 1,5-diazabicyclo[4.3.0]non-5-ene acetate ([DBNH][OAc]):DMSO = 50:50. The rheological properties of solutions were studied at temperatures 20–60 °C. Cellulose droplets formed under vibration were falling in ethanol coagulation bath forming alcogel beads, and the latter were dried with supercritical CO_2 resulting in cellulose aerogel beads. Cellulose solution jet, droplet and alcogel bead diameters, as well as size distribution of MCC- and viscose-based aerogel beads were measured and evaluated as a function of processing conditions (nozzle size, frequency of vibration, distance between the nozzle and coagulation bath and its temperature). Correlation parameter was used to rate the impact of the processing conditions on aerogel bead roundness and aspect ratio. Highly spherical aerogel beads (aspect ratio 1.09–1.16 and roundness 94.6–96.2) based on viscose- and MCC-based solutions were obtained with the nozzle size 400 µm, vibration frequency 100 Hz and nozzle-to-bath distance 3.5 cm. Their density was 0.08–0.12 $g.cm^{-3}$ and specific surface area around 400 $m^2.g^{-1}$. Cytotoxicity experiments demonstrated that both types of aerogels are harmless as tested on in vitro cultures.

Supplementary Information The online version contains supplementary material available at https://doi.org/10.1007/s10570-023-05659-x.

Introduction

In the view of current climate challenges and increasing pollution, the recycling and the demand for bio-based and biodegradable materials are constantly increasing. Textile industry has a significant environmental footprint using large areas of agricultural land and huge amount of water, energy and chemicals.

Additionally, fast-fashion trend increases the waste. Today, textile waste represents more than 92 million tons of materials globally discarded each year (Preferred Fiber and Materials Market Report - Textile Exchange 2022). It is mainly sent to open landfills or incinerated, and only 15% is reused and/or recycled, usually into materials of lower quality and functionality (mattress fillers, insulation mats), with only less than about 1% transformed back into yarn (Ellen MacArthur Foundation 2017). Thus, the European Commission has identified textiles as a priority product category within the circular economy approach (EU Strategy for Sustainable and Circular Textiles 2022). To move from a linear to a more circular and sustainable system, we need to go beyond collection of textile waste and downcycling.

One third of textile is entirely or partly composed of cellulose (cotton, viscose, Tencel, polycotton), which is the most abundant natural and biodegradable polymer on the Earth. Cellulose is a polysaccharide of choice in the development of sustainable and economically viable alternatives to replace products made of synthetic petroleum-based polymers. Till now, the upcycling options of cellulose-based textile are dissolving and spinning fibers or casting films (Haslinger et al. 2019). Recently, we suggested using cotton and viscose-based textile for making cellulose aerogels (Négrier et al. 2023), and a similar approach was also applied to denim (Zeng et al. 2019). Aerogels are low-density, open pores nanostructured materials with high specific surface area, at least above 100 $m^2.g^{-1}$ (Aegerter et al. 2023). Biopolymer-based aerogels have huge potential in various applications: for thermal and acoustic insulation (Zou and Budtova 2021; Budtova et al. 2023), in food and food packaging (Manzocco et al. 2021; Ciuffarin et al. 2023), as a catalyst and catalyst support (Rooke et al. 2011), for adsorption, absorption and separation (Zhang et al. 2016) and in pharmaceutical and bio-medical applications (García-González et al. 2021).

To make aerogels from cellulose-based textile, the latter should be first dissolved and, to this end, ionic liquids are powerful solvents that have been used to dissolve textile to spin fibers (Asaadi et al. 2016). 3D aerogel monoliths based on dissolved waste textile were made by adding a non-solvent to cellulose solution followed by drying with supercritical CO_2 (Zeng et al. 2019; Négrier et al. 2023). However, in many applications, aerogels as particles or beads are preferred (for example, as carriers of active substances): easy transportation and storage, high productivity rate and reduction of the whole process time and cost due to smaller dimensions is what industry is looking for (Ganesan et al. 2018). Various techniques can be applied to produce cellulose particles from a solution, resulting in diameter from a few microns to a few millimeters (Gericke et al. 2013). The techniques used are based either on dropping solution in a non-solvent (from a syringe Sescousse et al. 2011a; Trygg et al. 2013; Li et al. 2019), by spraying (Wang et al. 2014), jet cutting (Gavillon 2007; Druel et al. 2018; Schroeter et al. 2021), atomization (Callaghan et al. 2022)), or using emulsion/dispersion approach (Lin et al. 2009; Coombs OBrien et al. 2017; Omura et al. 2018; Druel et al. 2020). Prilling or laminar jet-breakup process is another efficient and easily scalable technique with high production rate used in chemical and pharmaceutical industries to produce micron-scaled particles (1–100 μm) with narrow size distribution (Sakai and Hoshino 1980). Fabrication of aerogel beads with prilling process have been reported for alginate (Del Gaudio et al. 2005) and pectin (De Cicco et al. 2016), but not for cellulose. The possibility to recycle and shape cellulose from textile waste into new high value-added materials at a large scale is a way to participate to circular economy.

To develop cellulose aerogels for a large range of applications, the toxicity of the final product should also be assessed. The toxicity of ionic liquids, in particular of the one used to spin fibers (Asaadi et al. 2016) and to make aerogels (Négrier et al. 2023), i.e. 1,5-diazabicyclo[4.3.0]non-5-ene acetate ([DBNH][OAc]), have rarely been addressed. Ruokonen et al. (2016) showed that [DBNH][OAc] is considered as harmless on hamster ovaries with a EC_{50} at 13,356 $mg.L^{-1}$ (Ruokonen et al. 2016). Witos et al. (2017) used phospholipids bilayers as models of natural bio-membranes with nanoplasmonic sensing at 0.25 M concentration (Witos et al. 2017); they also did not detect an effect of [DBNH][OAc] on the bio-membranes. Ruokonen et al. (2018) observed a low toxicity of [DBNH][OAc] since it did not induce any detectable changes within the bilayers even at 0.4 mM concentration (Ruokonen et al. 2018). Elsayed et al. (2020) investigated the toxicity of [DBNH][OAc] and its hydrolysis product, consisting of 1-(3-aminopropyl)-2-pyrrolidonium (APPH) and amide (Elsayed et al. 2020). EC_{50} was

also determined by measuring the decay of bioluminescence produced by *Vibrio Fischeri* bacteria. All compounds were classified as harmless with values between 3257 and 8322 mg/L after 5- and 15-min exposure.

In this work, we demonstrate the feasibility of producing cellulose "wet" and "dry" spherical particles via prilling. Cellulose aerogel beads were made from viscose textile and compared with beads from microcrystalline cellulose (MCC). Ionic liquid [DBNH][OAc] mixed with dimethyl sulfoxide (DMSO) was used as solvent, and drying with supercritical CO_2 was performed to preserve cellulose porosity. The influence of processing parameters on cellulose droplets' and aerogel beads' dimensions was investigated. Aerogels were characterized by density, specific surface area and morphology. Cytotoxicity of the viscose-based and MCC-based aerogels on human mesenchymal stem cells was assessed.

Experimental

Materials

Two types of cellulose were used: microcrystalline cellulose (MCC) Avicel® PH-101 purchased from Sigma-Aldrich and viscose textile (162 $g.m^{-2}$) purchased from Mondial Tissus. MCC is native cellulose (or cellulose I), and viscose is cellulose II, the latter was used to imitate waste textile. Cellulose degree of polymerization was determined from intrinsic viscosity (see Results section). In the following, "cellulose" will be used as a general term (for example, in Methods section), and "MCC-based" and "viscose-based" will be used when characterizing each specific solution or aerogel.

1,5-diazabicyclo[4.3.0]non-5-ene (DBN) was purchased from Fluorochem. Glacial acetic acid (purity > 99%) and dimethyl sulfoxide (DMSO) were from Fisher Scientific. Absolute ethanol (purity > 99%) was from Fisher Chemicals. Water was distilled. All chemicals were used as received.

For cytotoxicity assays, human bone marrow-derived mesenchymal stem cells (hMSCs) were purchased from Lonza. Alpha Minimum Essential Medium (α-MEM), phosphate buffered saline (PBS) and trypsin ethylenediaminetetraacetic acid (EDTA) were purchased from Sigma-Aldrich. Fetal bovine serum (FBS) and L-Glutamine were from Gibco. Cells tracers used for live/dead assays were ethidium homodimer-III (EthD-III) 1 mM in DMSO, calcein-AM and Hoechst 33,342, purchased from Biotium, In Vitrogen and Thermo Scientific, respectively. Methanol was purchased from Sigma-Aldrich. Sterile tissue culture plates of 48 wells with treated surface were from VWR.

Preparation of cellulose aerogel beads

Synthesis of ionic liquid

The ionic liquid ([DBNH][OAc]) was synthesized before each experiment as described elsewhere (Négrier et al. 2023). Briefly, glacial acetic acid and DBN were mixed in equimolar ratio (Ostonen et al. 2016). As the reaction is exothermal, acetic acid was slowly added to DBN under magnetic stirring and a cold-water bath was used to keep the temperature below 30 °C. After all acetic acid was added, the mixture was heated at 70 °C for 1 h to insure the complete reaction between the reagents. The obtained [DBNH][OAc] was transparent orange.

Cellulose dissolution and preparation of alcogel beads by prilling

Viscose textile was cut into 1–2 cm pieces and dispatched into fibers using a mixer. MCC and viscose were dried at 50 °C under vacuum for 3 h and each dissolved in 50/50 wt/wt [DBNH][OAc]/DMSO under magnetic stirring at 300 rpm for 24 h at room temperature (22 °C).

Droplets of solutions were formed using prilling tower (Spherisator M, BRACE—GmbH, Germany) with temperature controlled jacketed reactor (see Fig. 1). Depending on vibration frequency, around 80 to 150 droplets per minute can be produced. Temperature was fixed at 60 °C to have optimal solution viscosity, as will be discussed in Results section. The amplitude of the vibration was fixed at 2300 mV; pressure was adjusted according to nozzle diameter. A preliminary screening of prilling conditions was performed to select the parameters that provided visually spherical beads: the parameters selected are three nozzle diameters (300, 400 and 600 µm), three nozzle vibration frequencies (80, 100 and 150 Hz), three distances from the nozzle to the surface of coagulation

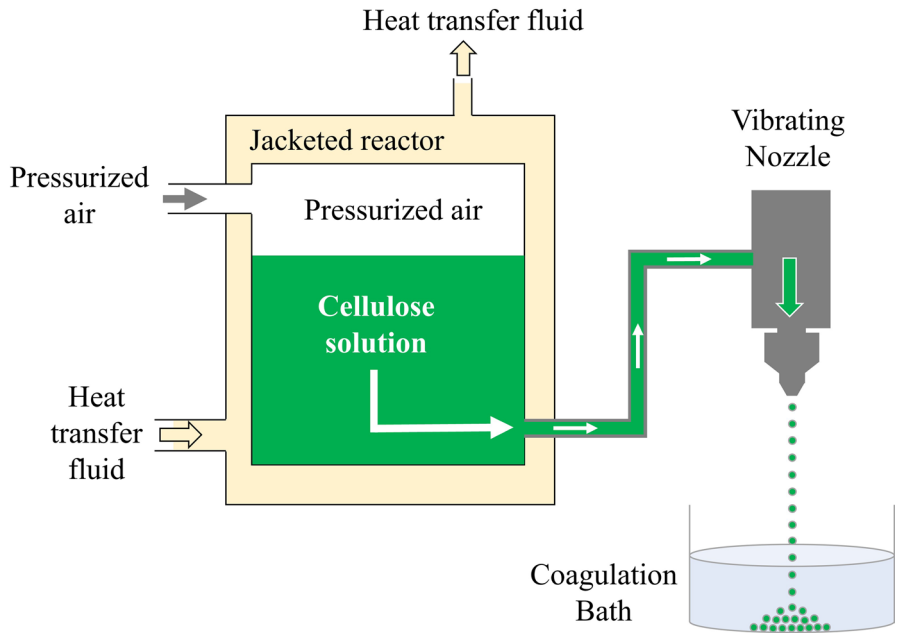

Fig. 1 A schematic presentation of a prilling tower and production of cellulose alcogel beads

bath (3.5, 6.5, and 9.5 cm) and three coagulation bath temperatures (10, 20 and 30 °C). The mass flow rate of the extruded liquid was measured over a minute and was used to deduce the volumetric flow rate. Solution droplets were falling in ethanol (cellulose non-solvent) leading to cellulose coagulation and formation of alcogel beads (Fig. 1). Ethanol was used as it is miscible with [DBNH][OAc]/DMSO and with CO_2, the latter used for drying in supercritical conditions. Before drying, coagulated cellulose beads were washed in ethanol to remove the ionic liquid/DMSO. To ensure a complete replacement of the ionic liquid by ethanol, the electric conductivity of the bath was monitored.

Supercritical CO_2 drying

Drying of alcogel beads with supercritical CO_2 was performed as described elsewhere (Négrier et al. 2023). Briefly, beads were placed in 1 L autoclave, pressurized under CO_2 at 50 bar and 37 °C and ethanol purged. Then, the pressure was increased to 80 bar to reach the supercritical conditions of CO_2. The system was kept under these conditions during 1 h with an output of 5 kg of CO_2/h to perform a dynamic washing and remove the remaining ethanol from the alcogels. After this cycle, the system was left in a static mode for 1–2 h and another dynamic cycle of washing for 2 h was repeated. The depressurization was carried out with a ramp of 4 bar/h at 37 °C.

Characterization

Determination of cellulose degree of polymerization (DP)

The intrinsic viscosity *[η]* (mL.g^{-1}) of microcrystalline cellulose and viscose was measured by cellulose dissolution in cupriethylenediamine (CED), following the SCAN-CM standard 15:88 containing the requirements of the ISO 5351. The LAUDA iVisc equipped with an Ubbelohde-type viscometer was used. The molecular weight M was determined from Mark-Houwink-Sakurada equation:

$$[\eta] = K \times M^a = K' \times DP^a \quad (1)$$

where $a = 0.90$ and $K = 1.65$ are empirical constants reported by Evans and Wallis (Evans and Wallis 1989). We used the $K' = 0.606$ mL.g^{-1} to calculate the DP.

Rheology of cellulose-[DBNH][OAc]/DMSO solutions

Bohlin Gemini rheometer (Malvern Instruments) with a Peltier plate for temperature control and plate-plate

geometry (plates of 60 mm diameter, gap 1 mm) was used. All experiments were performed within maximum a week after solvent and solutions preparation. Temperature was varied from 10 to 60 °C. For the steady state mode, shear rate was varied from 0.01 to 1000 s^{-1}. For dynamic mode, frequency sweeps were performed within 0.01 Hz and 10 Hz at 5 Pa, corresponding to the linear viscoelastic regime. Because ionic liquids absorb humidity from air, a thin layer of silicon oil (η(20 °C) = 9.5 mPa.s) was applied on the edges of the measuring cell to prevent moisture and oxygen uptake.

Analysis of the jet and droplets' dimensions

Droplets falling into the coagulation bath were recorded with Pointgrey Grasshopper3 camera (GS3-U3-41C6M-C, 4.1MP, 90 FPS). Snapshots were made and used to measure the average diameter of the jet d_{jet} close to the nozzle exit and of four droplets per jet of which a mean value was calculated, d_{drop}. Considering the droplets as spheres before they enter the coagulation bath (See Figure S1 in the Supporting Information), their volumes were then deduced and used to calculate the shrinkage from droplet to aerogel bead.

Analysis of aerogel beads' dimensions, shape and size distribution

The shape, dimensions, and size distribution with the span of aerogels beads were obtained by analyzing the images of beads taken in transmitted light using Visilog software; it provides the length and width of each bead, and an equivalent diameter D automatically calculated from the bead surface (100–200 beads analysed per formulation).

The distribution of D in volume was determined for each processing condition. Volume distribution was chosen instead of number distribution to obtain more information about the larger beads. In addition, a three-point specification, i.e. the span in D volume distribution, was used as an indicator to analyze the width of the size distribution. This value gives the "distance" between the points located at 10 and 90 percent of distribution, normalized with the midpoint. The closer is the span to zero, the more uniform is the equivalent diameter distribution. The span is defined as:

$$Span = \frac{\left(D_{90} - D_{10}\right)}{D_{50}} \tag{2}$$

where D_{90}, D_{50}, and D_{10} are the mean diameters of the beads cumulatively counted at 90, 50, and 10% in volume, respectively.

Circularity is one of the main parameters to characterize the bead shape. The classical way to calculate circularity is to consider particle area and perimeter (Eq. 3):

$$Circularity = 4\pi \times \frac{Area}{Perimeter^2} \tag{3}$$

In order to take into account the bead aspect ratio (AR), Takashimizu (Takashimizu and Iiyoshi 2016) suggested an equation for the "roundness" R (Eq. 4):

$$R = Circularity + \left(Circularity_{\text{perfect circle}} - Circularity_{\text{aspect ratio}}\right) \tag{4}$$

where $Circularity_{\text{perfect circle}} = 0.913$ (and not 1.0 because digital images comprise an aggregate of pixels and include errors (Takashimizu and Iiyoshi 2016)), and

$$\begin{aligned} Circularity_{\text{aspect ratio}} = {} & 0.826261 + 0.337479\,AR \\ & - 0.335455\,AR + 0.103642\,AR^3 \\ & - 0.0155562\;AR^4 + 0.00114582\,AR^5 \\ & - 0.0000330834\,AR^6 \end{aligned} \tag{5}$$

with the aspect ratio AR defined as:

$$AR = \frac{L}{W} \tag{6}$$

where L is the length and W the width of the bead.

A correlation analysis was performed to rate processing parameters (nozzle-to-bath distance, bath temperature, nozzle diameter and frequency of vibration) that have the most significant impact and positively or negatively influence beads' equivalent diameter, roundness, and aspect ratio. This method assesses a possible two-way linear association between two variables, measured by the Pearson correlation coefficient, dimensionless, taking a value in the range from − 1 to + 1. Zero, the median value, indicates that there is no linear correlation between the two variables. A positive and a negative correlation means that both variables move in the same direction or in opposite directions, respectively (Mukaka 2012).

Characterization of aerogel beads

The volume shrinkage during the preparation of aerogel beads was calculated as follows:

$$Shrinkage(\%) = (1 - \frac{V_{\text{final,1}}}{V_{\text{initial}}}) \times 100 \quad (7)$$

where V_{initial} and $V_{\text{final,1}}$ are the volumes of the droplet of cellulose solution falling in the bath (see Sect. 2.3.4) and of the aerogel bead respectively. The volume of aerogel bead was calculated using the equivalent diameter.

The bulk (or envelope) density (ρ_{bulk}) of aerogels was determined as the ratio of sample mass (m) to volume ($V_{\text{final,2}}$):

$$\rho_{bulk}(g.cm^{-3}) = \frac{m}{V_{\text{final,2}}} \quad (8)$$

where "sample mass" is the weight of a dozen beads measured with high-precision balance and $V_{\text{final,2}}$ is their total volume determined using GeoPyc 1360 Envelope Density Analyzer (Micromeritics) with DryFlo powder, chamber of 19.1 mm diameter and the applied force 27 N. The experimental error did not exceed 3%.

The porosity and the theoretical specific pore volume v_{pores} were calculated from the bulk and skeletal density ($\rho_{\text{sk}} = 1.5$ g.cm^{-3} (Sun 2005)) as follows:

$$Porosity(\%) = (1 - \frac{\rho_{\text{bulk}}}{\rho_{\text{sk}}}) \times 100 \quad (9)$$

$$v_{pores}(cm^3.g^{-1}) = \frac{1}{\rho_{\text{bulk}}} - \frac{1}{\rho_{\text{sk}}} \quad (10)$$

The specific surface area (S_{BET}) was measured with the ASAP 2020 High-Performance Adsorption Analyzer (Micromeritics), using nitrogen adsorption technique and Brunauer–Emmett–Teller (BET) approach. The samples were first degassed under high vacuum at 70 °C for 12 h. The average error was below 20 m^2.g^{-1}. Pore size distribution and pore volume in the range of mesopores and small macropores was obtained using Barret-Joyner-Halenda (BJH) approach and nitrogen sorption/desorption data.

The morphology of the surfaces and of the cross-sections of cellulose aerogel beads was analyzed with Scanning Electron Microscopy (SEM) using a MAIA 3 (Tescan), equipped with detectors of secondary and back-scattered electrons. A 14 nm layer of platinum was applied with a Q150T Quarum metallizer to prevent the accumulation of electrostatic charges and images' defaults. The observations were done with an acceleration voltage set at 3 kV.

Cytotoxicity assays on aerogel

Cellulose aerogel discs based on MCC or on viscose were prepared mimicking the procedure for making aerogel beads: cellulose solutions were casted in a 48-well culture plates, coagulated and washed with ethanol. Then each alcogel cylinder was cut with a vibrating blade microtome (Leica VT1000 S) into thin disks and dried with supercritical CO_2. The obtained aerogel discs had a diameter of 8 mm and a thickness of 1 mm and were sterilized by UV light for 1.5 h.

Before the experiment, hMSCs were cultured in a T75-flask to passage 5 in α-MEM, supplemented with 10 vol% of FBS, 2 mM of L-Glutamine, 100 U/mL of penicillin and 100 µg/mL of streptomycin, at 37 °C in a humidified atmosphere containing 5% CO_2. The supplemented α-MEM will be called α-MEMc.

The cytotoxicity assay was performed using conditioned medium. It was prepared by incubating MCC- and viscose-based aerogel discs for 24 h at 37 °C and 5% CO_2 in α-MEMc. Before confluence, hMSCs were seeded at a concentration of 3 100 cells. cm^{-2} in α-MEMc in a 48-well plate. After 4 h, the medium was replaced by 24 h-conditioned α-MEMc and hMSCs cultured for 10 days with conditioned α-MEMc change every 3 days with respective medium (3 days-MCC-based aerogel conditioned, 3 days-viscose-based aerogel conditioned α-MEMc and α-MEMc). Live/dead staining was performed at 1, 3, 7 and 10 days by incubating the cells in a α-MEMc containing calcein (4 µM), Hoechst (1 µg. mL^{-1}) and ethidium (2 mM) at 37 °C for 20 min in the dark. Wells were then briefly rinsed with PBS prior fluorescent imaging performed with an inverted microscope (Carl Zeiss™ Axio Vert.A1 with Axiocam 202 mono). Excitations wavelengths were 385, 475 and 555 nm for Hoechst, calcein and ethidium stains, respectively. A minimum of 15 images at × 5 magnification were taken for each condition. Green (alive) and red (dead) stained hMSCs were counted using the image analysis software ImageJ. A per cent of viability was calculated as a ratio of the number of

green stained hMSCs and the total of hMSCs (stained in green and red). Positive and negative controls were performed and consisted of hMSCs cultured with non-conditioned media, and hMSCs cultured with non-conditioned media and exposed to 70% methanol in PBS prior to staining as per manufacturer protocol, respectively. Five technical replicates were used.

Results and discussion

Determination of microcrystalline cellulose and viscose degree of polymerization

Intrinsic viscosity values and the corresponding DP (see Characterization section) of MCC and viscose are presented in Table 1. The DP of MCC is 248 and of viscose 384, which is consistent with the values reported in literature (Négrier et al. 2023; Druel et al. 2018; Kadolph and Langford 2010).

Rheological properties of MCC- and viscose-based [DBNH][OAc]/DMSO solutions

The rheological properties of cellulose dissolved in imidazolium-based ionic liquids, neat (Druel et al. 2018; Gericke et al. 2009; Sescousse et al. 2010) or mixed with DMSO (Lv et al. 2012; Saba et al. 2015), as well as in neat [DBNH][OAc] (Hummel et al. 2015) had already been reported. All systems show classical polymer solution behavior. To the best of our knowledge, viscoelastic properties of cellulose dissolved in [DBNH][OAc]/DMSO have not been studied. A detailed study of the rheological properties of cellulose/[DBNH][OAc]/DMSO solution was not the goal of this work; below the steady state and dynamic rheology is presented for the solutions used for making beads.

Figure 2 (a, b) shows viscosity as a function of shear rate and Fig. 2 (c, d) of dynamic moduli as a function of frequency ω for MCC (Fig. 2a, c) and viscose (Fig. 2b, d) dissolved in 50/50 [DBNH][OAc]/DMSO. As expected, viscosity decreases with temperature increase, and it is higher for viscose-based solutions compared to MCC-based solutions. Figure 2a, b shows that the flow of all solutions, in particular, of MCC solutions, is Newtonian in a large interval of shear rates. In the linear viscoelastic region (Fig. 2c, d) all solutions fully obey Maxwell model, with elastic modulus $G' \sim \omega^{1.9-2}$ and viscous modulus $G'' \sim \omega^{0.95-0.98}$. Cox-Mertz approach is demonstrated in the Supporting Information, Figure S2; it shows that steady state and dynamic viscosities coincide for solutions of the same cellulose type at the same temperature. Moreover, the Arrhenius approach was applied for MCC and viscose solutions; the Newtonian viscosity (η_N) vs temperature is shown in Figure S3. The activation energy was 32 and 34 kJ.mol^{-1} for MCC- and viscose-based solutions, respectively, calculated from the slope of the curves, all showing linear trends ($r^2 > 0.99$). Higher activation energy values of 52 and 54 and 64 kJ.mol^{-1} were reported by Sescousse et al. for 5 wt% MCC-[EMIM][OAc] and MCC-[BMIM][Cl] solutions, respectively, and by Druel et al. for 5 wt% MCC-[DBNH][CO_2Et] solutions; however, those solutions were in ionic liquids without any co-solvent added (Sescousse et al. 2010; Druel et al. 2018).

A preliminary screening (not shown) demonstrated that in order to obtain more or less spherical droplets using prilling, solution viscosity should be between 0.1 and 0.4 Pa.s. Considering that i) to make self-standing cellulose aerogels polymer concentration should be at least twice higher than the overlap concentration (for MCC it is around 1–1.5 wt% in a similar solvent (Gericke et al. 2009)) and ii) high solution temperatures should be avoided to prevent cellulose degradation and unwanted chemical reactions, solutions of 5 wt% MCC/[DBNH][OAc]/DMSO and 4 wt% viscose/[DBNH][OAc]/DMSO at 60 °C were selected, with viscosity equal to 0.19 and 0.32 Pa.s, respectively.

Table 1 Intrinsic viscosity and DP of all celluloses used in the work

Cellulose source	MCC	Viscose
Intrinsic viscosity (mL.g^{-1})	86.5 ± 1.7	128.4 ± 2.6
DP	248 ± 5	384 ± 8

Analysis of cellulose solution droplets' dimensions

First, we checked if classical theories developed for other polysaccharide solutions (e.g., alginate) falling in a gelation bath (Serp et al. 2000; Cramer et al. 2004) can be applied to MCC- and viscose-based

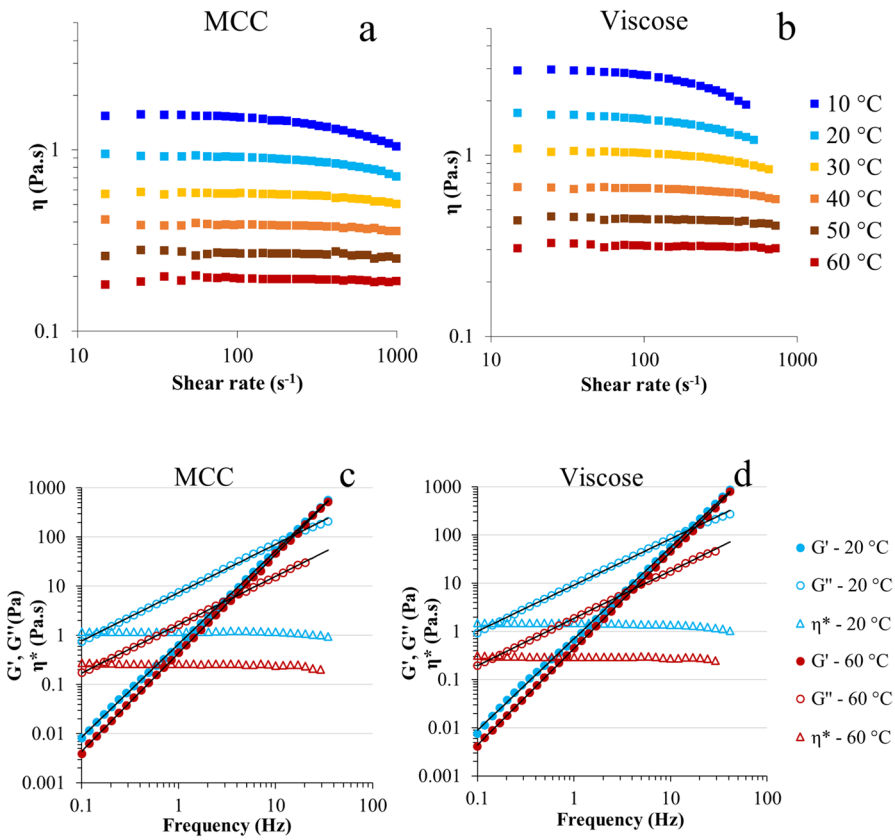

Fig. 2 Viscosity as a function of shear rate (**a**, **b**) and elastic modulus (G'), viscous modulus (G'') and complex viscosity (η*) as a function of frequency (**c**, **d**) for solutions of 5 wt% MCC (**a**, **c**) and 4 wt% viscose (**b**, **d**), each dissolved in 50/50 [DBNH][OAc]/DMSO. Solid lines are power law approximations for dynamic moduli

solutions. The measured wavelength λ was compared with calculated one for different processing conditions (Cramer et al. 2004):

$$\lambda = \frac{U}{f} \tag{11}$$

where U is jet velocity corresponding to the selected nozzle diameter and f the vibrational frequency. For both MCC and viscose solutions the calculated and measured wavelengths are very similar, as shown in Figure S4a, b, and thus calculated wavelength will be in the following used for simplicity.

The diameter of the jet, d_{jet}, and of cellulose solution droplets produced by prilling, d_{drop}, were measured experimentally (see Sect. 2.3.3) and also calculated using the approaches developed in (Serp et al. 2000):

$$d_{jet\ calc} = \left[\frac{4.F}{\pi.f.\lambda}\right]^{1/2} \tag{12}$$

$$d_{drop\ calc} = (1.5 d_{jet}^2 \lambda)^{1/3} \tag{13}$$

where F is the volumetric flow rate of the extruded liquid. Droplet diameter can be then simply calculated as follows (Serp et al. 2000):

$$d_{drop\ calc} = \left[\frac{6.F}{\pi.f}\right]^{1/3} \tag{14}$$

Measured jet diameters and droplet diameters are compared to their calculated values in Figs. 3 and 4, respectively, and show excellent fit for MCC solution and reasonably good fit for viscose solution. Prilling (or jet-vibrating) technique can thus be easily applied to form droplets of cellulose solutions (of low and medium molecular weight) which diameter can be easily predicted.

It should be noted that small satellite droplets were also produced during prilling process in addition to the primary droplets (Cramer et al. 2004). Satellite droplets of cellulose solution with a volume below 10% of the primary droplet are created

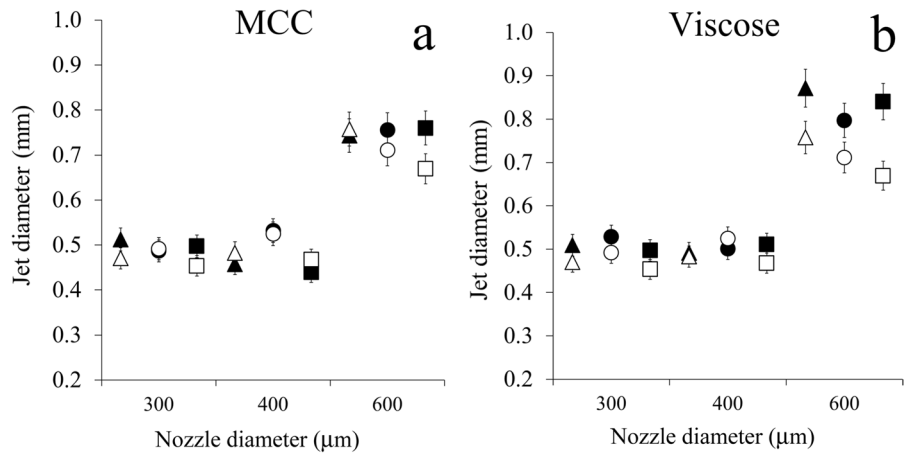

Fig. 3 Comparison of the measured (filled) and calculated (open) jet diameter using Eq. 12, for MCC (**a**) and viscose (**b**) solutions for various prilling conditions: frequency 80 Hz (triangles), 100 Hz (circles) and 150 Hz (squares) and nozzle diameter 300, 400 and 600 µm

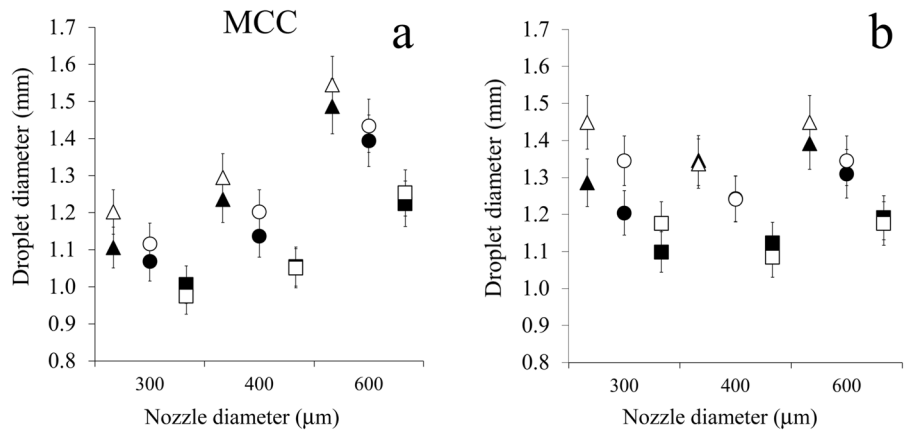

Fig. 4 Comparison of the measured (filled) and calculated (open) droplet equivalent diameter using Eq. 13, for MCC (**a**) and viscose (**b**) solutions for various prilling conditions: frequency 80 Hz (triangles), 100 Hz (circles) and 150 Hz (squares) and nozzle diameter 300, 400 and 600 µm

when the air applies drag force on the primary cellulose droplet. First, neck-breaking occurs, which corresponds to the elongation and the split of the solution jet between the new formed droplet and the nozzle. Then, the recoiling jet is broken due to high capillary pressure generating satellite droplets. Parameters such as the increase of velocity and flow rate of the jet or the low surface tension of the solution tend to produce more satellite droplets. It was also demonstrated that the influence of solution viscosity on the droplet size was negligible as compared to the flow rate of the jet (Cramer et al. 2004). However, a high viscosity combined with a high flow rate and high velocity increase the length of the neck, and satellite droplets formation is enhanced (5–15% in number).

Analysis of aerogel beads' dimensions and selection of the optimal processing conditions

For every prilling parameters combinations, the distributions in volume of MCC- and viscose-based aerogel beads' equivalent diameter are represented in Fig. 5. For both MCC and viscose-based aerogels, the beads made using 400 µm nozzle show a narrower equivalent diameter distribution compared to the 300 and 600 µm counterparts. Moreover, equivalent diameter distribution for viscose-based aerogel beads (0.75–1.25 mm) is narrower than that for MCC-based (0.75–1.55 mm). Overall, the 400 µm nozzle size seems the most appropriate to obtain narrower aerogel bead equivalent diameter distribution while the 600 µm nozzle leads to a wider bead equivalent diameter distribution.

The values of span are presented in Figure S5 in the Supporting Information as a function of

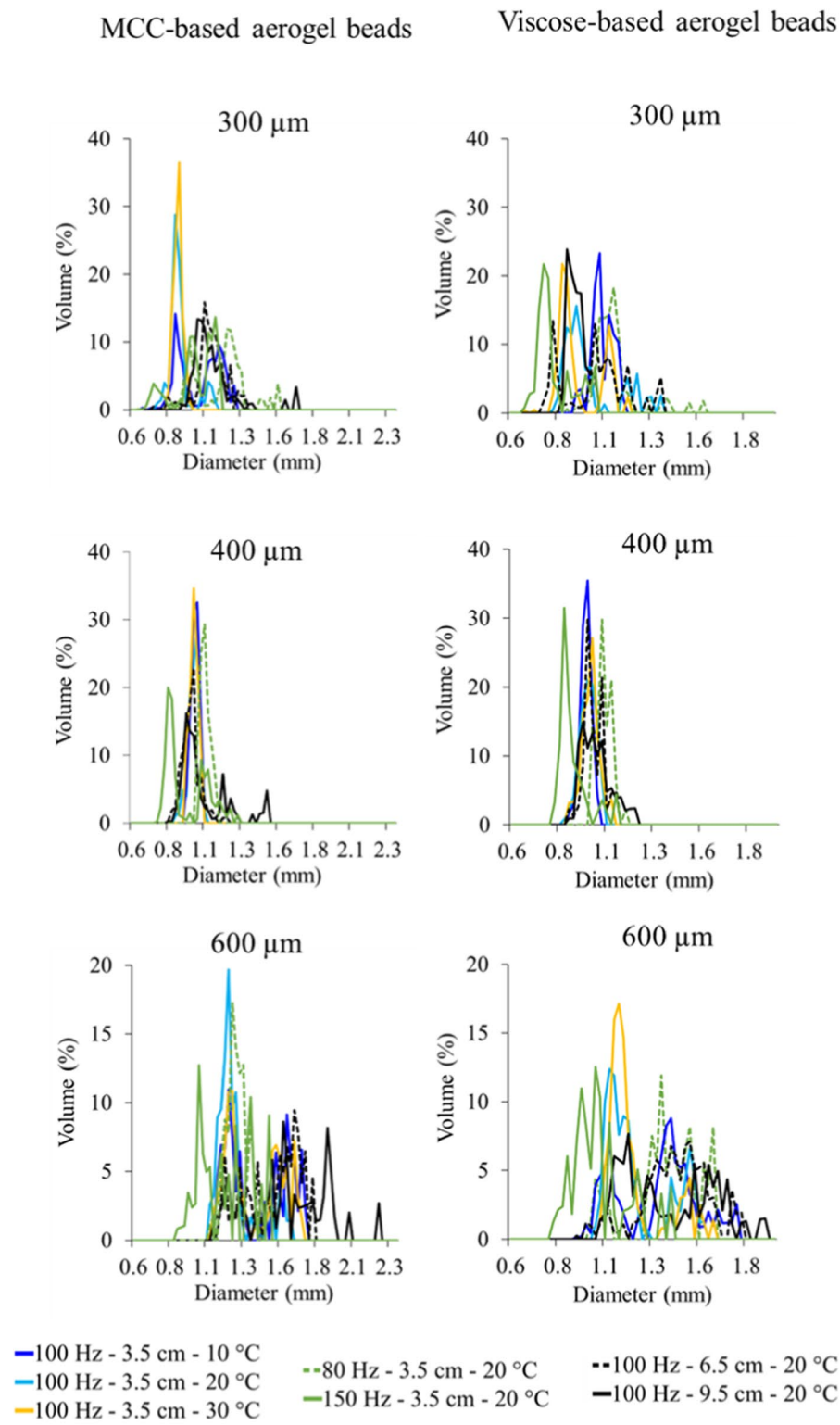

Fig. 5 MCC- and viscose-based aerogel bead equivalent diameter distributions in volume for various nozzle diameters, frequencies, nozzle-to-bath distances, and bath temperatures

frequency, nozzle-to-bath distance, and bath temperature, each for three values of nozzle diameter. No clear trend of the span as a function of process parameters can be deduced, however, practically in all cases, the 400 µm nozzle diameter results in the lowest span values.

All results obtained in this work for bead mean equivalent diameter, aspect ratio, roundness and span are presented in Table S1 in the Supporting Information. In green we mark the highest roundness value (> 95%), the lowest aspect ratio (< 1.15) and the lowest span (< 1.12); in red are the "worst" results in terms of lowest roundness, the highest aspect ratio, and the highest span.

The correlation coefficients analysis (see details in Figure S6 in the Supporting Information) shows that for both MCC and viscose beads, the equivalent diameter is highly impacted by the nozzle diameter, followed by the frequency of vibration, then to a lesser extent by the nozzle-to-bath distance. The aspect ratio of beads is mainly driven by the nozzle-to-bath distance and the frequency, followed by the nozzle-to-bath distance. The roundness of beads seems to be correlated only with the nozzle diameter and the frequency of vibration. Finally, the temperature of the coagulation bath does not show any significant impact on these three parameters. The increase of the nozzle diameter obviously increases the equivalent diameter but also the aspect ratio while decreasing the roundness leading to less spherical beads. The increase of the frequency of vibration logically decreases the beads diameter (since the cellulose solution jet is more often cut) and it also decreases the roundness with the increase of the aspect ratio, so the beads are less spherical. As expected, the increase of the nozzle-to-bath distance increases the diameter of the beads and the aspect ratio due to the flattening of the droplet of cellulose solution, but not the roundness.

Table 2 summarizes an example of the best results in terms of aerogel beads' highest roundness and lowest aspect ratio. They correspond to the "optimal conditions" which are nozzle with diameter 400 µm, vibration frequency 100 Hz, nozzle-to-bath distance 3.5 cm and bath temperature of 20 °C. Since temperature does not have any significant impact on the beads parameters, both 10 and 30 °C are also considered as "optimal conditions" but to facilitate the interpretation, the results obtained at 20 °C only will be discussed. Moreover, high roundness coupled with a low aspect ratio can also be observed for the 300 µm beads for a frequency of 100 Hz, a nozzle-to-bath distance of 3.5 cm at 30 °C (Table S1). Beads obtained with the nozzle diameter 600 µm do not present good characteristics since their mean roundness was lower or just above 95% (Table S1).

Table 2 Summary of the best results (taken from Table S1) corresponding to mean roundness at optimal conditions: frequency 100 Hz, 400 µm nozzle diameter and the 3.5 cm nozzle-to-bath distance, at 20 °C

	5 wt% MCC-based	4 wt% viscose-based
Average bead equivalent diameter (mm)	0.98	0.96
Average bead length *L* (mm)	1.06	1.06
Average bead width *W* (mm)	0.97	0.93
Aspect ratio *L/W*	1.09	1.13
Roundness *R*	0.97	0.98

The illustration of aerogel beads length, width and roundness distributions corresponding to the "optimal conditions" (400 µm nozzle diameter, 3.5 cm nozzle-to-bath distance, vibration frequency of 100 Hz and bath temperature 20 °C) is presented in Fig. 6 for MCC- and viscose-based aerogel beads. Length and width (Fig. 6a, c) show narrow distributions around 1 mm, and more than 94% of the beads (Fig. 6b, d) show a very high roundness, > 95%, for both MCC- and viscose-based aerogel beads. An example of "non-optimal conditions" are presented in Figure S7 in the supporting information.

Characterization of aerogel beads

The representative examples of alcogel and aerogel beads are shown on Fig. 7, and dry aerogel beads with spherical (from optimal conditions) and ellipsoidal (non-optimal conditions) shapes are shown on Fig. 8. The characteristics of MCC-based and viscose-based aerogel beads (300 µm–100 Hz–3.5 cm and 20 °C) are presented in Table 3; they are very similar and also similar to their monolithic counterparts (Négrier et al. 2023). Viscose-based aerogel beads are of a slightly lower density than that of MCC-based aerogels due to the lower polymer concentration in the starting solution; consequently, the porosity and specific pore

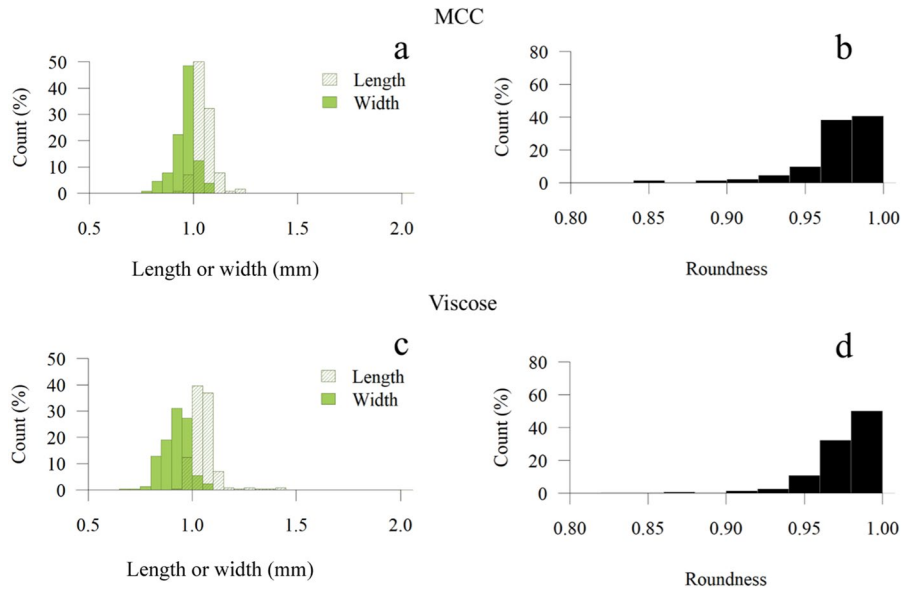

Fig. 6 MCC- (**a**, **b**) and viscose-based (**c**, **d**) aerogel beads length and width (**a**, **c**), and roundness (**b**, **d**) distributions for the "optimal conditions": 400 µm nozzle diameter, bath temperature 20 °C, 3.5 cm nozzle-to-bath distance and vibration frequency 100 Hz

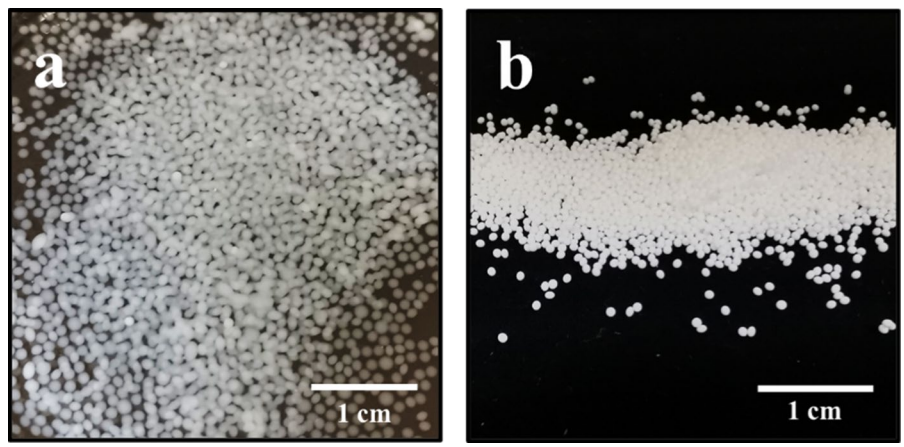

Fig. 7 Viscose-based alcogel beads (**a**) and the corresponding aerogel beads (**b**)

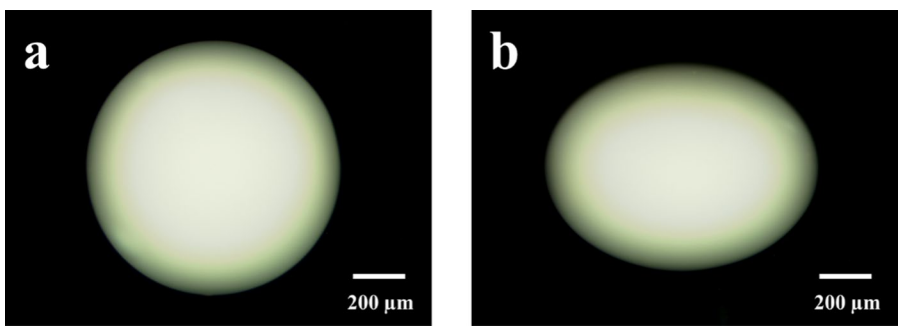

Fig. 8 Optical microscope images of viscose-based aerogel beads obtained with optimal conditions (**a**): 300 µm–100 Hz–3.5 cm and 20 °C and non-optimal conditions (**b**): 600 µm–100 Hz–6.5 cm–30 °C

Table 3 Characteristics of MCC- and viscose-based aerogel beads (300 µm–100 Hz–3.5 cm and 20 °C): total shrinkage, bulk density, porosity, specific pore volume and specific surface area

Aerogel beads	MCC-based	Viscose-based
Total shrinkage (%)	42 ± 5	47 ± 5
Bulk density ($g.cm^{-3}$)	0.115 ± 0.003	0.084 ± 0.002
Porosity (%)	93 ± 3	97 ± 3
Specific pore volume ($cm^3.g^{-1}$)	8.4 ± 0.3	11.8 ± 0.4
Specific surface area ($m^2.g^{-1}$)	416 ± 20	398 ± 20

volume of viscose-based aerogel beads are slightly higher than those of MCC-based counterparts.

The surface and inner morphology of viscose-based aerogel beads is presented in Fig. 9. Instantaneous liquid–liquid demixing occurring when cellulose droplet was in contact with the non-solvent and further shrinkage resulted in the formation of a wavy skin layer (Fig. 9a); this layer is porous on a nanoscale (Fig. 9b). The inner morphology (Fig. 9c, d) is typical to aerogels made from cellulose dissolved in ionic liquids and/or their mixtures with DMSO and coagulated directly in a non-solvent, without initial solution gelation (Sescousse et al. 2011b; Buchtová and Budtova 2016; Pircher et al. 2016; Négrier et al. 2023): it is a network of assembled "hairy" beads formed due to spinodal decomposition-governed phase separation.

BJH approach was used to test if it can be applied for the determination of aerogels' pores size distribution. An example of sorption/desorption dependence is shown in Figure S8 in the Supporting Information. Specific pore volume given by this approach is 1.2 $cm^3.g^{-1}$ while the same determined from bulk and skeletal density (Eq. 10) is 11.8 $cm^3.g^{-1}$ (see Table 3). BJH approach covers only 10% of the total pore volume; similar results were obtained for other bio-aerogels (Robitzer et al. 2013; Groult and Budtova 2018). Pore size distribution calculated from BJH approach is shown in Figure S9: the peak is at 46 nm and median is at 42 nm corresponding to pore diameters in the meso- and small macropores regions. These values are not representative as this pore size distribution does not cover all pores' dimensions in cellulose aerogels.

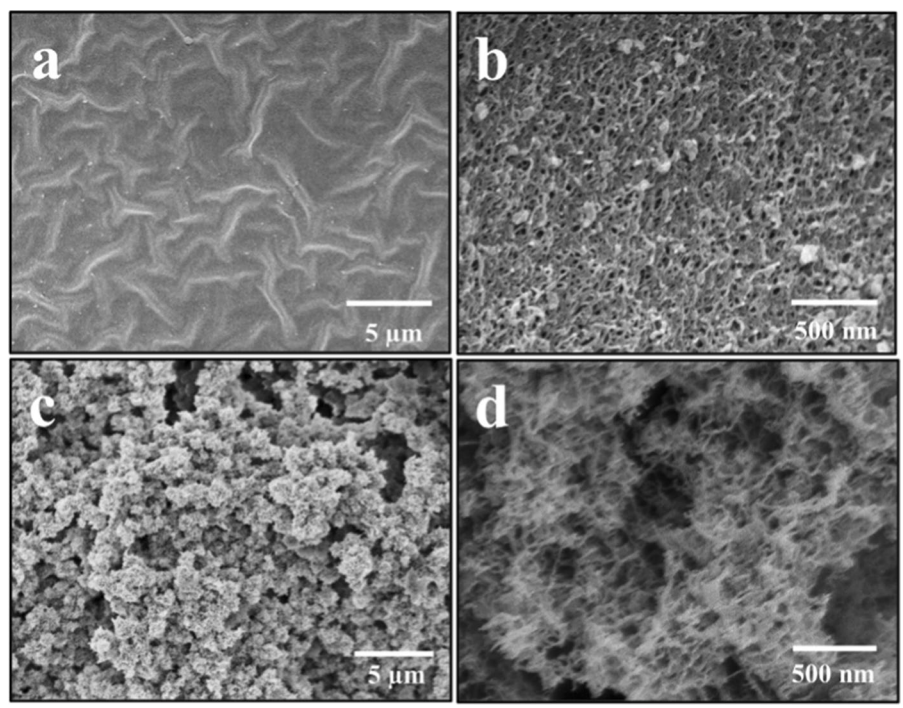

Fig. 9 SEM observation of the outer (**a**, **b**) and inner (**c**, **d**) morphology of the viscose-based aerogel beads

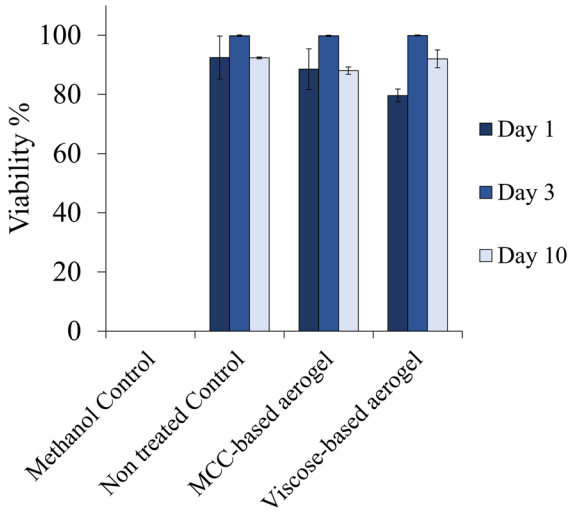

Fig. 10 Viability of hMSCs in media conditioned with MCC and viscose aerogels after 1, 3, 7 and 10 days

Cytotoxicity of aerogels

In vitro viability of hMSCs in the presence of media conditioned with MCC and viscose-based aerogels was investigated over a 10-day period (Fig. 10). Qualitatively, a very high cell viability above 75% at day 1 and 90% at day 10 was observed for all conditions.

The morphology of hMSCs cultured in media conditioned with MCC and viscose aerogels was similar to the positive control (non-treated) consisting of normal culture medium except at day 10 when the hMSCs showed a tendency for a reduced density (decrease of around 20%) and less spread cells in the media conditioned with the aerogels. This suggests an impact of aerogels leach out products on hMSCs ability to attach and proliferate (Fig. 11). Further investigations are required to characterize the leach-out and their effect on hMSCs.

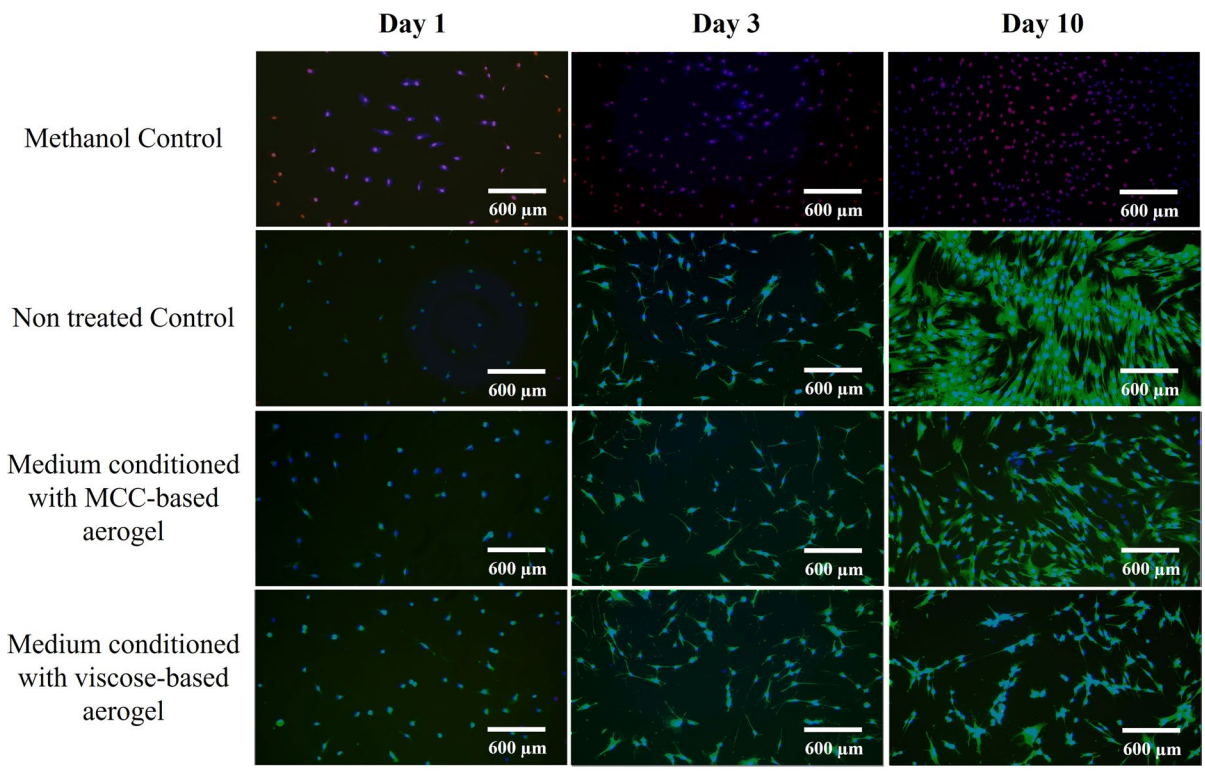

Fig. 11 Morphology of hMSCs in media conditioned with MCC and viscose over 10 days

Conclusions

Aerogel beads based on viscose textile and on microcrystalline cellulose dissolved in ionic liquid ([DBNH][OAc]:DMSO = 50:50) were prepared using prilling (or jet-vibrating) technique and characterized. The rheological properties of the starting solutions were investigated to select cellulose concentration leading to reasonably spherical beads. Solutions showed classical viscoelastic behaviour with Newtonian flow in a large region of shear rates.

Cellulose solution jet and bead diameter of cellulose coagulated in ethanol (alcogel) was measured and calculated using approaches developed for the droplets of other polysaccharides. Measured and theoretical values showed an excellent fit, allowing the prediction of the final alcogel bead size as a function of prilling parameters (nozzle size, frequency of vibration).

Aerogels were made from cellulose alcogel beads via drying with supercritical CO_2. Correlations between processing conditions and aerogel bead roundness and aspect ratio were built. It was demonstrated that nozzle diameter has the main impact on aerogel bead dimensions, followed by the frequency of vibration, and then by the nozzle-to-bath distance. Bath temperature, used from 20 to 60 °C, practically does not have any influence on aerogel bead roundness and aspect ratio. Optimal conditions to obtain the narrowest aerogel bead equivalent diameter distribution were with the nozzle size 400 µm, a vibration frequency 100 Hz, a nozzle-to-bath distance 3.5 cm. Highly spherical aerogel beads based on MCC- and viscose-based solutions were of diameter around 1 mm and with low aspect ratio 1.09–1.16 and very high roundness 94.6–96.2. The properties and inner morphology of aerogel beads showed characteristics similar to their monolithic counterparts (Négrier et al. 2023): density 0.08–0.12 $g.cm^{-3}$ and specific surface area around 400 $m^2.g^{-1}$. Finally, media conditioned with MCC- and viscose-based aerogels do not affect hMSCs viability in vitro.

This work opens new pathways for textile recycling and making high-added value materials. Prilling was shown to be an attractive way of producing cellulose particles (whatever is cellulose source, cellulose I or II) which can be used as carriers for controlled release or as matrices for absorption or adsorption.

Acknowledgments Authors are grateful to Institut CARNOT M.I.N.E.S for funding and ANR, "Investissements d'Avenir" program, ANR-18-EURE-0021 project, for labeling. We warmly thank Julien Jaxel (PERSEE, Mines Paris, France) for supercritical drying, Antoine Perron (RAPSODEE, IMT Mines Albi, France) for the help in prilling process, Christophe Pradille (MatXper, France) for providing beads' analysis equipment, Romain Castellani (CEMEF, Mines Paris, France) for the guidance in the rheological measurements and Alain Corinus (IPMC, CNRS, France) for the cutting of the samples for cytotoxicity tests.

Author contributions M.N.: Conceptualization, Data curation, Formal Analysis, Investigation, Methodology, Writing—original draft, Writing—review & editing; E.E.A.: Funding acquisition, Writing—review & editing; R.S.: Funding acquisition, Writing—review & editing; M.S.: Funding acquisition, Writing—review & editing; G.B.: Conceptualization, Data curation, Formal Analysis, Validation, Writing—review & editing; D.E., Conceptualization, Formal Analysis, Validation, Writing—review & editing; T.B.: Conceptualization, Formal Analysis, Funding acquisition, Investigation, Methodology, Project administration, Resources, Supervision, Validation, Writing—original draft, Writing—review & editing.

Funding This project has received funding from Institut CARNOT MINES.

Data availability Data are available upon request.

Declarations

Conflict of interests No competing interests.

Ethical approval Not applicable.

Consent to participate Not applicable.

Consent for publication All authors agree to publish the results presented in the article.

References

Aegerter MA, Leventis N, Koebel M, Steiner III SA (2023) Handbook of Aerogels, 2nd edition. Springer Nature Switzerland AG, 1800 pages

Asaadi S, Hummel M, Hellsten S et al (2016) Renewable high-performance fibers from the chemical recycling of cotton waste utilizing an ionic liquid. Chemsuschem 9:3250–3258. https://doi.org/10.1002/cssc.201600680

Buchtová N, Budtova T (2016) Cellulose aero-, cryo- and xerogels: towards understanding of morphology control. Cellulose 23:2585–2595. https://doi.org/10.1007/s10570-016-0960-8

Budtova T, Lokki T, Malakooti S, Rege A, Lu H, Milow B, Vapaavuori J, Sl V (2023) Acoustic properties of aerogels: current status and prospects. Adv Eng Mater 25:2201137. https://doi.org/10.1002/adem.202201137

Callaghan C, Scott JL, Edler KJ, Mattia D (2022) Continuous production of cellulose microbeads by rotary jet atomization. J Colloid Interface Sci 627:1003–1010. https://doi.org/10.1016/j.jcis.2022.07.120

Ciuffarin F, Négrier M, Plazzotta S, Libralato M, Calligaris S, Budtova T, Manzocco L (2023) Interactions of cellulose cryogels and aerogels with water and oil: Structure-function relationships. Food Hydrocolloids 140:108631. https://doi.org/10.1016/j.foodhyd.2023.108631

Coombs OBrien J, Torrente-Murciano L, Mattia D, Scott JL, (2017) Continuous Production of Cellulose Microbeads via Membrane Emulsification. ACS Sustain Chem Eng 5:5931–5939. https://doi.org/10.1021/acssuschemeng.7b00662

Cramer C, Fischer P, Windhab EJ (2004) Drop formation in a co-flowing ambient fluid. Chem Eng Sci 59:3045–3058. https://doi.org/10.1016/j.ces.2004.04.006

De Cicco F, Russo P, Reverchon E, García-González CA, Aquino RP, Del Gaudio P (2016) Prilling and supercritical drying: A successful duo to produce core-shell polysaccharide aerogel beads for wound healing. Carbohyd Polym 147:482–489. https://doi.org/10.1016/j.carbpol.2016.04.031

Del Gaudio P, Colombo P, Colombo G, Russo P, Sonvico F (2005) Mechanisms of formation and disintegration of alginate beads obtained by prilling. Int J Pharm 302:1–9. https://doi.org/10.1016/j.ijpharm.2005.05.041

Druel L, Niemeyer P, Milow B, Budtova T (2018) Rheology of cellulose-[DBNH][CO2Et] solutions and shaping into aerogel beads. Green Chem 20:3993–4002. https://doi.org/10.1039/C8GC01189C

Druel L, Kenkel A, Baudron V, Buwalda S, Budtova T (2020) Cellulose aerogel microparticles via emulsion-coagulation technique. Biomacromol 21:1824–1831. https://doi.org/10.1021/acs.biomac.9b01725

Ellen MacArthur Foundation (2017) A New Textiles Economy: Redesigning fashion's future. Available from: https://ellenmacarthurfoundation.org/a-new-textiles-economy

Elsayed S, Hellsten S, Guizani C, Witos J, Rissanen M, Rantamäki AH, AH, Varis P, Wiedmer SK, Sixta H, (2020) Recycling of superbase-based ionic liquid solvents for the production of textile-grade regenerated cellulose fibers in the lyocell process. ACS Sustain Chem Eng 8:14217–14227. https://doi.org/10.1021/acssuschemeng.0c05330

EU Strategy for Sustainable and Circular Textiles. Communication from the commission to the European parliament, the council, the European economic and social committee and the committee of the regions. Brussels, 30.3.2022 https://environment.ec.europa.eu/publications/textiles-strategy_en. Accessed 27 Apr 2023

Evans R, Wallis AFA (1989) Cellulose molecular weights determined by viscometry. J Appl Polym Sci 37:2331–2340. https://doi.org/10.1002/app.1989.070370822

Ganesan K, Budtova T, Ratke L, Gurikov P, Baudron V, Preibisch I, Niemeyer P, Smirnova I, Milow B (2018) Review on the Production of Polysaccharide Aerogel Particles. Materials 11:2144. https://doi.org/10.3390/ma11112144

García-González CA, Sosnik A, Kalmár J, Jozsef Kalmar J, De Marco I, Erkey C, Concheiro A, Alvarez-Lorenzo C (2021) Aerogels in drug delivery: From design to application. J Control Release 332:40–63. https://doi.org/10.1016/j.jconrel.2021.02.012

Gavillon R (2007) Preparation and characterization of ultra porous cellulosic materials. PhD thesis, Mines ParisTech

Gericke M, Schlufter K, Liebert T, Heinze T, Budtova T (2009) Rheological properties of cellulose/ionic liquid solutions: from dilute to concentrated states. Biomacromol 10:1188–1194. https://doi.org/10.1021/bm801430x

Gericke M, Trygg J, Fardim P (2013) Functional cellulose beads: preparation, characterization, and applications. Chem Rev. https://doi.org/10.1021/cr300242j

Groult S, Budtova T (2018) Thermal conductivity/structure correlations in thermal super-insulating pectin aerogels. Carbohyd Polym 196:73–81. https://doi.org/10.1016/j.carbpol.2018.05.026

Haslinger S, Hummel M, Anghelescu-Hakala A, Määttänen M, Sixta H (2019) Upcycling of cotton polyester blended textile waste to new man-made cellulose fibers. Waste Manag 97:88–96. https://doi.org/10.1016/j.wasman.2019.07.040

Hummel M, Michud A, Asaadi S, Ma Y, Hauru LKJ, Hartikainen E, Sixta H (2015) Rheological Requirements for Continuous Filament Spinning of Cellulose-Ionic Liquid Solutions

Kadolph SJ, Langford AL (2010) Textiles, 11th edn. Pearson

Li B, Pan Y, Zhang Q, Huang Z, Liu J, Xiao H (2019) Porous cellulose beads reconstituted from ionic liquid for adsorption of heavy metal ions from aqueous solutions. Cellulose 26:9163–9178. https://doi.org/10.1007/s10570-019-02687-4

Lin C, Zhan H, Liu M, Fu SY, Lucia LA (2009) Novel preparation and characterization of cellulose microparticles functionalized in ionic liquids. Langmuir 25:10116–10120. https://doi.org/10.1021/la9008703

Lv Y, Wu J, Zhang J, Niu Y, Liu CY, He J, Zhang J (2012) Rheological properties of cellulose/ionic liquid/dimethylsulfoxide (DMSO) solutions. Polymer 53:2524–2531. https://doi.org/10.1016/j.polymer.2012.03.037

Manzocco L, Mikkonen KS, García-González CA (2021) Aerogels as porous structures for food applications: Smart ingredients and novel packaging materials. Food Struct 28:100188. https://doi.org/10.1016/j.foostr.2021.100188

Mukaka M (2012) A guide to appropriate use of Correlation coefficient in medical research. Malawi Med J 24:69–71

Négrier M, Ahmar E, Sescousse R, Sauceau M, Budtova T (2023) Upcycling of textile waste into high added value cellulose porous materials, aerogels and cryogels. RSC Sustainability. https://doi.org/10.1039/D2SU00084A

Omura T, Imagawa K, Suzuki T, Minami H (2018) Morphology control of porous cellulose particles by tuning the surface tension of media during drying. Langmuir 34:15490–15494. https://doi.org/10.1021/acs.langmuir.8b03422

Ostonen A, Bervas J, Uusi-Kyyny P, Alopaeus V, Zaitsau DH, Emel'yanenko VN, Schick C, King AWT, Helminen J, Kilpeläinen I, Khachatrian AA, Varfolomeev MA, Verevkin SP (2016) Experimental and Theoretical Thermodynamic Study of Distillable Ionic Liquid 1,5-Diazabicyclo[4.3.0]non-5-enium Acetate. https://doi.org/10.1021/ACS.IECR.6B02417

Pircher N, Carbajal L, Schimper CB, Bacher M, Rennhofer H, Nedelec JM, Lichtenegger HC, Rosenau T, Liebner F (2016) Impact of selected solvent systems on the pore and

solid structure of cellulose aerogels. Cellulose. https://doi.org/10.1007/s10570-016-0896-z

Preferred Fiber and Materials Market Report - Textile Exchange. (2022) https://textileexchange.org/preferred-fiber-and-materials-market-report/. Accessed 25 Jan 2023

Robitzer M, Di Renzo F, Quignard F (2013) Natural materials with high surface area. Physisorption methods for the characterization of the texture and surface of polysaccharide aerogels. Microporous Mesoporous Mater. https://doi.org/10.1016/j.micromeso.2010.10.006

Rooke J, Matos Passos C, Chatenet M, Sescousse R, Budtova T, Berthon-Fabry S, Mosdale R, Maillard F (2011) Synthesis and properties of platinum nanocatalyst supported on cellulose-based carbon aerogel for applications in PEMFCs. J Electrochem Soc 158:B779–B789. https://doi.org/10.1149/1.3585744

Ruokonen S-K, Sanwald C, Sundvik M, Polnick S, Vyavaharkar K, Duša F, Holding AJ, King AWK, Kilpeläinen I, Lämmerhofer M, Panula P, Wiedmer SK (2016) Effect of ionic liquids on Zebrafish (Danio rerio) viability, behavior, and histology; correlation between toxicity and ionic liquid aggregation. Environ Sci Technol 50:7116–7125. https://doi.org/10.1021/acs.est.5b06107

Ruokonen S-K, Sanwald C, Robciuc A, Hietala S, Rantam-ki AH, Witos J, King AWT, Lammerhofer M, Wiedmer SK (2018) Correlation between Ionic Liquid Cytotoxicity and Liposome-Ionic Liquid Interactions. Chemistry 24:2669–2680. https://doi.org/10.1002/chem.201704924

Saba H, Yongbo Y, Jianning W, Xiaolin X, Kaijian W, Yumei Z, Huapinga W (2015) Effect of dimethylsulfoxide on the viscoelastic properties and sol–gel transition of cellulose/ionic liquid solutions. RSC Adv 5:8318–8322. https://doi.org/10.1039/C4RA14911D

Sakai T, Hoshino N (1980) Production of uniform droplets by longi-tudinal vibration of audio frequency. J Chem Eng Jpn 13:263–268. https://doi.org/10.1252/jcej.13.263

Schroeter B, Yonkova VP, Niemeyer NAM, Jung I, Preibisch I, Gurikov P, Smirnova I (2021) Cellulose aerogel particles: control of particle and textural properties in jet cutting process. Cellulose 28:223–239. https://doi.org/10.1007/s10570-020-03555-2

Serp D, Cantana E, Heinzen C, Von Stockar U, Marison IW (2000) Characterization of an encapsulation device for the production of monodisperse alginate beads for cell immobilization. Biotechnol Bioeng 70:41–53

Sescousse R, Le KA, Ries ME, Budtova T (2010) Viscosity of Cellulose−Imidazolium-Based Ionic Liquid Solutions. J Phys Chem B 114:7222–7228. https://doi.org/10.1021/jp1024203

Sescousse R, Gavillon R, Budtova T (2011a) Wet and dry highly porous cellulose beads from cellulose–NaOH–water solutions: influence of the preparation conditions on beads shape and encapsulation of inorganic particles. J Mater Sci 46:759–765. https://doi.org/10.1007/s10853-010-4809-5

Sescousse R, Gavillon R, Budtova T (2011b) Aerocellulose from cellulose–ionic liquid solutions: Preparation, properties and comparison with cellulose–NaOH and cellulose–NMMO routes. Carbohyd Polym 83:1766–1774. https://doi.org/10.1016/j.carbpol.2010.10.043

Sun C, (Calvin), (2005) True density of microcrystalline cellulose. J Pharm Sci 94:2132–2134. https://doi.org/10.1002/jps.20459

Takashimizu Y, Iiyoshi M (2016) New parameter of roundness R: circularity corrected by aspect ratio. Prog in Earth and Planet Sci 3:2. https://doi.org/10.1186/s40645-015-0078-x

Trygg J, Fardim P, Gericke M, Mäkilä E, Salonen J (2013) Physicochemical design of the morphology and ultrastructure of cellulose beads. Carbohydr Polym 93:291–299. https://doi.org/10.1016/j.carbpol.2012.03.085

Wang Q, Fu A, Li H, Liu J, Guo P, Zhao XS, Xia LH (2014) Preparation of cellulose based microspheres by combining spray coagulating with spray drying. Carbohyd Polym 111:393–399. https://doi.org/10.1016/j.carbpol.2014.05.002

Witos J, Russo G, Ruokonen S-K, Wiedmer SK (2017) Unraveling Interactions between Ionic Liquids and Phospholipid Vesicles Using Nanoplasmonic Sensing. Langmuir 33:1066–1076. https://doi.org/10.1021/acs.langmuir.6b04359

Zeng B, Wang X, Byrne N (2019) Development of cellulose based aerogel utilizing waste denim—A Morphology study. Carbohyd Polym 205:1–7. https://doi.org/10.1016/j.carbpol.2018.09.070

Zhang H, Li Y, Xu Y et al (2016) Versatile fabrication of a superhydrophobic and ultralight cellulose-based aerogel for oil spillage clean-up. Phys Chem Chem Phys 18:28297–28306. https://doi.org/10.1039/C6CP04932J

Zou F, Budtova T (2021) Polysaccharide-based aerogels for thermal insulation and superinsulation: An overview. Carbohyd Polym 266:118130. https://doi.org/10.1016/j.carbpol.2021.118130